Robust Attenuated Total Reflection Infrared Spectroscopic Sensors Based on Quantum Cascade Lasers for Harsh Environments

Andrea Teuber and Boris Mizaikoff, *Member, IEEE*

***Abstract*—A compact yet robust sensor system for applications in harsh environments has been developed. The sensor takes advantage of infrared attenuated total reflection (IR-ATR) spectroscopy with an invariant coupling of IR radiation into the ATR sensing element via substrate-integrated hollow waveguides (iHWGs). The system design, which is supported by appropriate simulations, minimizes the influence of environmental parameters (e.g., hydrostatic pressure, mechanical vibrations, etc.) at the optically delicate ATR waveguide. Next to an innovative radiation coupling concept via iHWGs in lieu of conventional optics, IR-transparent fibers were used. The fibers ensure a direct optical connection of the quantum cascade laser (QCL) light source and the detector to the iHWG coupling elements of the sensor cell.**

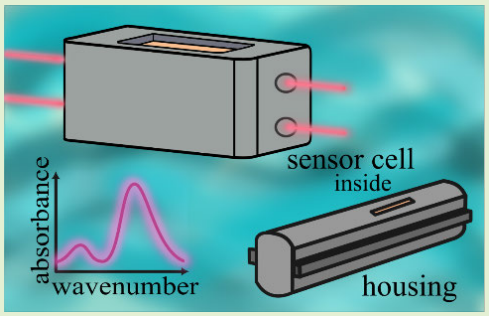

***Index Terms*— Attenuated total reflection (ATR), harsh environments, midinfrared (MIR), quantum cascade laser (QCL), sensor design, substrate-integrated hollow waveguide (iHWG).**

I. Introduction

IN THE past years, the need for protecting and saving the environment became increasingly evident, e.g., due to observable and imminent climate change. This need leads to an enhanced demand for monitoring and detecting associated environmental changes. Especially in marine systems, additional pollution may arise from oil and fuel industry or natural oil spill events. Oil is then spread naturally across large areas via wind and waves and followed by emulsification or entrapment of crude oil in selected zones of sea water. Other sensing scenarios include but are not limited to sensing dissolved gases in the deep sea (e.g., in CO_2 geo-sequestration scenarios) and water resource management [1], [2], [3], [4], [5], [6], [7], [8], [9], [10], [11], [12]. Besides pollution, the marine environment itself may lead to problems for marine infrastructures, cultural artifacts, and so on, for example, via corrosion and biocorrosion events. At such occasions, spontaneous processes occur due to the presence of chlorides and dissolved oxygen and may be further enhanced by the presence of (electro)chemically active microorganisms. Thus, these microorganisms—especially bacteria and algae—may colonize metallic surfaces by forming biofilms, and consequently, corrosion of the metal occurs [13]. However, such microorganism and their metabolism/proliferation may be affected by temperature changes in the marine environment [14]. Therefore, materials that can withstand such corrosion processes are needed to be used in these harsh environments. For example, VA4 stainless steel [15] is an ideal choice to be used in harsh environment, as it is resistant against many forms of corrosion. Furthermore, besides corrosion and temperature effects in the marine environment, the movement of the water mass and the hydrostatic pressure must be taken into account, especially if delicate sensor systems are operated at such harsh conditions.

If an external force is applied onto a body, the internal resistance per unit area of body can be expressed as stress. Stress is defined as two fundamental types, i.e., tensile (positive) and/or compressive (negative) [16], [17]. The stress to strain in a material is called modulus of elasticity or Young's modulus. It explains the compressibility of a material or the stiffness of a solid material. Increasing the modulus of elasticity leads to a less compressible body [16], [18]. The yield stress is the minimum applied stress that will cause a solid to undergo a

Manuscript received 4 October 2023; accepted 24 October 2023. Date of publication 13 November 2023; date of current version 2 January 2024. This work was supported in part by the European Union's Horizon 2020 Research and Innovation Program under Grant 101094818 (TRIQUETRA). The associate editor coordinating the review of this article and approving it for publication was Prof. Subhas C. Mukhopadhyay. *(Corresponding author: Boris Mizaikoff.)*

Andrea Teuber is with the Institute of Analytical and Bioanalytical Chemistry, Ulm University, 89081 Ulm, Germany (e-mail: andrea.teuber@uni-ulm.de).

Boris Mizaikoff is with the Institute of Analytical and Bioanalytical Chemistry, Ulm University, 89081 Ulm, Germany, and also with Hahn-Schickard, 89077 Ulm, Germany (e-mail: boris.mizaikoff@uni-ulm.de).

Digital Object Identifier 10.1109/JSEN.2023.3330525

permanent deformation or plastic flow. The latter represents the transition from elastic to plastic behavior [19]. Combining all individual stress components, the Von Mises criterion is obtained. It is based on yield stress in uniaxial tension and shear forces in the plane and a measure for the "state of the stress" [16], [20]. When the Von Mises stress exceeds the yield strength, ductile materials start to deform. This in turn correlates with a change in shape indicating the intensity of the stress relative to the yield strength [21], [22], [23]. Another strain parameter is the Poisson ratio, which occurs if a force is applied onto a material, and the material contracts in lateral direction. Therefore, pulling a dense material leads to a linear elastic range of deformation and a slight decrease in volume [16], [24], [25]. Zinc selenide (ZnSe), a typical attenuated total reflection (ATR) waveguide material, which is used in the present infrared (IR) sensor concept, shows a steep elastic increase in stress followed by a work-hardening after yielding [26].

Midinfrared (MIR) spectroscopy is a nondestructive and versatile analytical method providing molecularly characteristic vibrational signatures of analytes. MIR spectroscopy can be used to analyze liquids (e.g., aqueous) solutions, semi-soft materials (e.g., gels and pastes), or solid materials (e.g., powders) next to gas phase constituents. The usual spectral working range extends from 4000 to 400 cm^{-1} (2.5 to 25 μm) and has the benefit-in comparison to far-infrared (FIR) and near-infrared (NIR) spectroscopy—that the so-called "fingerprint region" (>8 μm) provides unique signatures for almost any organic and/or inorganic molecule [27], [28], [29], [30]. In ATR spectroscopy, an internal reflection element (IRE) made from IR-transparent materials—herein, ZnSe with a higher refractive index compared to the adjacent medium—is used as an active transducer. IR radiation propagates along the IRE via total internal reflection, if the critical angle is surpassed [29]. As a result, an evanescent field emanates at these reflection points, which leaks with exponentially decaying intensity several micrometers into the adjacent medium. The interaction between the evanescent field and the sample results in a wavelength-dependent attenuation of the IR radiation [31]. The evanescent field leakage can be calculated using the penetration depth (d_p). The latter is dependent on the ratio of the refractive indices of the IRE (n_1) and the surrounding medium (n_2), the wavelength (λ) of the radiation, and the angle of incidence (θ) [32], [33], [34], [35], as shown in the following:

$$d_p = \frac{\lambda}{2\pi \left(n_1^2 \sin^2 \theta - n_2^2\right)^{1/2}}. \quad (1)$$

In routine analysis, and especially in laboratory scenarios, Fourier transform infrared (FTIR) spectrometers are usually applied [27]. FTIR devices cover the entire MIR range. However, they provide a limited energy density per wavelength [36], [37] and are usually less sensitive in comparison to laser-based spectroscopies, e.g., quantum cascade laser (QCL) light sources operating in the MIR. QCLs provide an exceptional energy density per wavelength, albeit in a limited spectral window. In addition to emissive power, operation in continuous or pulse mode on chip dimensions and tailorability across the entire MIR band are distinct advantages of QCLs. In particular, the potential for miniaturization and battery operation promises laser-based IR spectroscopy and sensing as a particularly useful technology for portable devices [30]. Corresponding miniaturized sensors are especially needed in on-site and in situ environmental analysis scenarios, where online and/or in-field monitoring are the main goal. Furthermore, such sensors have to be shock and vibration resistant and sufficiently robust to be operated in harsh environments [5], [14], [15].

Conventionally, water analysis techniques rely on sampling (i.e., automated or manual sample collection), sample storage in suitable containers, whereby any interaction between sample constituents and container has to be avoided [38]. Besides sample collection and storage, sample transport and sample preparation processes in the laboratory are critical and may affect the composition of the sample [39].

Herein, we present a compact and exceedingly robust IR-ATR sensor interface integrated into a field-deployable housing. The proposed sensor is specifically designed for operation in harsh environment while taking advantage of conventional MIR waveguides, such as ZnSe crystals, yet packaged such that they withstand vibrations and shocks. The developed sensor cell is based on a generic concept that may be combined with any IR laser light source and detection scheme. All sensing elements can be placed inside a specifically designed cylindrical housing for portable operation. To prove the robustness of the developed sensor system for environmental analysis, pressure simulations were performed. Additionally, experimental studies using model analyte confirm the utility of the developed sensor cell.

II. Compact Sensor System for Environmental Monitoring: Innovative IR-ATR Sensor Design

A. Design of a Robust IR-ATR Transducer Assembly

The herein presented IR-ATR sensor interface is an advanced design based on previous studies by our research team (see [31]). The sensor and its individual components are shown in Fig. 1. The design can be considered a "sandwich structure" composed of two individual subunits [see Fig. 1(a) and (c)]. Each unit can host an individual ZnSe IRE. The presence of two independent compartments provides several advantages and increased versatility: 1) one of the cells can be used for measuring reference analytes without the need of exchanging solutions; 2) two different analytes can be analyzed simultaneously, if individual lasers are used that target individual analyte absorptions; 3) different environments can be simultaneously investigated; and 4) changes in the sensor cell (e.g., failure of one sensor cell) during operation do not limit its utility given the obtained redundancy.

The symmetrically designed sandwich parts are separated by a hollow-core reference channel. This reference channel can be used to determine fluctuations of the laser light source as the light passes through without any sample interaction. On top of the reference channel, a stainless-steel holder with a mechanically thinned lead plate is installed. This holder has an "H" shape, and at the crossbar, a lead plate with the same dimension as the ZnSe crystal is located. Lead is used

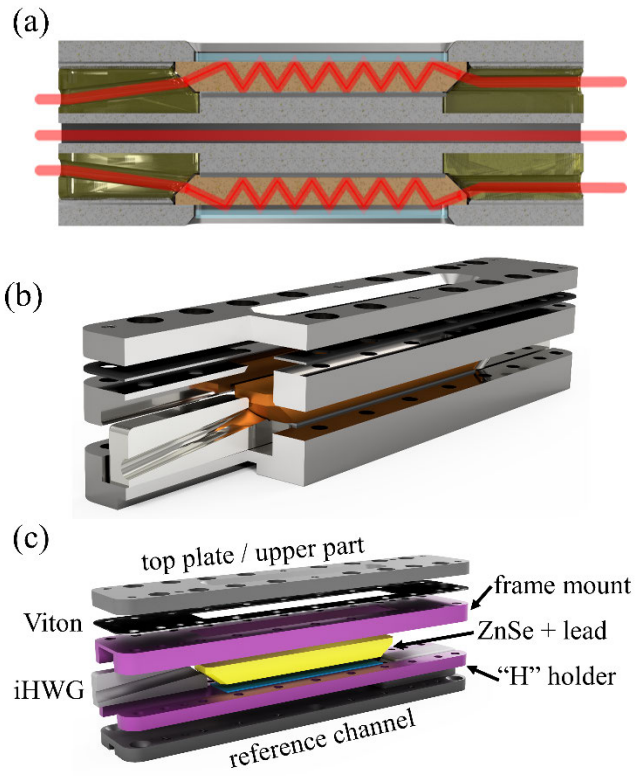

Fig. 1. Developed sensor cell is composed of individual components, which can be tailored to any desired measurement scenario in terms of materials and dimensions. (a) Schematic of the transducer assembly. In red, the laser beam is schematically shown indicating the internal reflections within the ATR waveguide. IR radiation is guided *via* iHWGs to the IRE and *via* another iHWG to the detector. (b) CAD rendering illustrating the iHWG coupling. (c) Labeling of the individual parts, which are used for establishing the sensor cell assembly.

for providing a reasonably soft yet robust embedment for the ZnSe crystal. This crystal serves as the active transducer with dimensions of 72 × 6 × 10 mm (l × w × h) providing several internal reflections and a sufficient large active sensing area. The ZnSe IRE is framed at both end facets by individual substrate-integrated hollow waveguides (iHWGs) serving as invariable radiation coupling elements.

iHWGs, first developed by Mizaikoff and coworkers [40], serve in the present sensor design as a direct optical coupling element. This coupling element delivers IR laser radiation to the IRE and from its distal end to the detector. Due to the invariable structure, the system is permanently aligned without the need of adjustable optics. Lenses, for example, can be avoided, as the iHWGs focus the radiation onto the crystal end facet without any option for misalignment (e.g., due do vibrations/shock changing the position of lenses) or even breakage of optical elements. The iHWG couplers are fabricated via 3-D printing (Formlabs Form 3, Formlabs, USA) and tailored individually to the IRE coupling facets (see Fig. 1). In a more sophisticated version, they may of course be fabricated from aluminum or stainless steel. The iHWGs are also designed to protect the fragile corners of the IRE while maximizing the incoupling efficiency.

To mount the ZnSe crystal and the iHWGs in position in the y-direction, an additional component serves as a frame-shaped

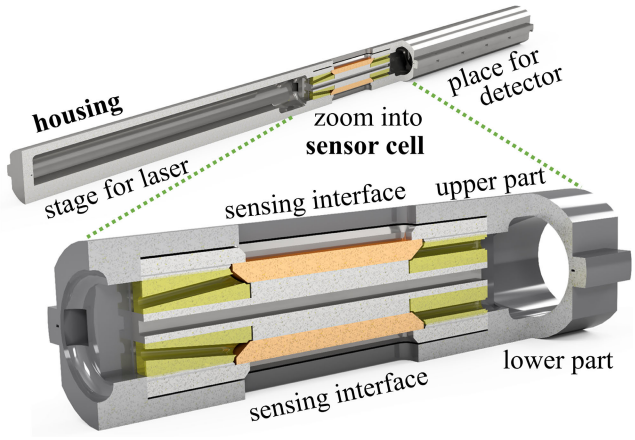

Fig. 2. IR-ATR transducer assembly inserted into the system housing. The system housing comprises two hemi-cylindrical parts sealed via an O-ring with an outer tube diameter of 5 cm after assembly.

mount, as evident in Fig. 1(b) and (c). The frame-shaped part has a cutout with the dimensions of the IRE crystal. Due to the shape of this frame, the iHWGs and the IRE are pressed against the lead sheet at the ground plate (i.e., the "H"-shaped part). It also protects and covers the ZnSe crystal in y-direction [see Fig. 1(b)].

For sealing purposes, a Viton sheet is used. It is located between the frame mount and the top plate [see Fig. 1(c)]. The upper part closes the sensor from the top and also serves as the liquid sample chamber with a volume of approx. 1 mL. However, the sample volume may be individually tailored to the need of the application. As the IRE is fully embedded into the sensor cell, the assembly is ideally suited for high-fluid-pressure applications. No free optical path is present and no moving parts or parts that may misalign at harsh conditions are used. Furthermore, no additional lenses and mirrors are needed within the entire assembly. The overall dimensions of the transducer system are 130 × 25 × 37 mm (l × w × h).

B. Construction of a System Housing for the IR-ATR Sensor Cell

A system housing has been developed, again ensuring a possibly robust and compact design. The dimensions are <1 m in length with an outer system diameter of 5 cm, which is the smallest achievable diameter using the present transducer assembly. The cylindrical system housing (see Fig. 2) comprises two individual parts—an upper and lower substrate—which are sealed against each other via screw mounts along the wing-shaped structures extending to the left and right of the housing half-cylinders. Inside the wings, an O-Ring is used for sealing purposes. Each half is fabricated from a stainless steel VA4 block. The transducer assembly is designed such to precisely and modularly (i.e., exchangeable) fit the cutout of the system housing, as shown in Fig. 2.

All optical and electronical components, such as lasers and detectors, are located inside this tubular housing. Connecting the iHWG couplers to the laser light source(s) and to the detector(s) via fiberoptic cables avoids any free space radiation propagation within the entire system.

The system is optically designed, such that 1) the QCL housing is already mounted at the optical axis of the iHWG couplers and 2) that heat is efficiently dissipated from the laser. The design of the internal "optical bench" allows for mounting several lasers in series along the central axis of the device. Each laser is then coupled *via* individual fiberoptic cables to the iHWG inside the sensor cell. At the distal end the housing system, mounts for small IR detectors are provided, e.g., thermopiles. Since less space is needed for the detector, the sensor housing is not symmetrically constructed, i.e., the detector compartment is smaller compared to the laser compartment. Furthermore, both ends of the tube provide connectors for delivering the required electric power into the sensor housing. Space for cables is designed between the sensor cell and the connection wings, such that future additional electrical components may be added.

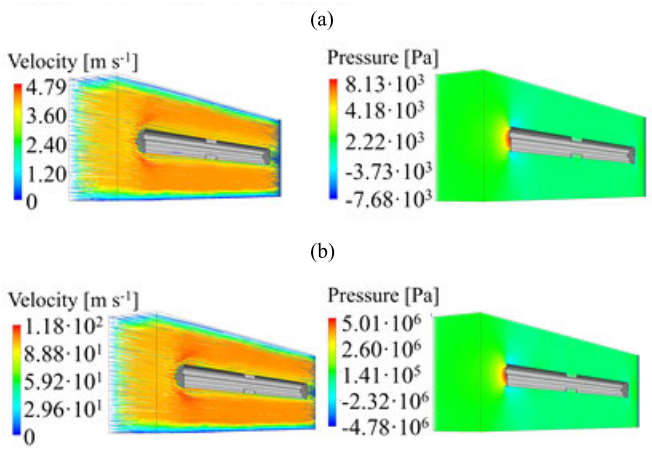

Fig. 3. Simulations of water flow. (a) Flow velocity of 4 m/s and (b) flow velocity of 10 m/s.

C. Sensor Design Considerations for Operation in Harsh Environments

As shown in Figs. 1 and 2, while the sensor system appears quite complex, it is easy to assemble given the modularity of the concept. The system was designed, such that even untrained personnel without special tools may assemble the device. The main goal was to establish a versatile (i.e., not limited to any environment) and compact system with the potential to use a variety of light sources, yet primarily MIR lasers. Physical parameters to be considered are the sensor design, coupling to the transducer, and effects of pressure, shock, temperature, and vibrations. Since marine environments accelerate corrosion, VA4 stainless steel was selected as the core material. However, Ti or Ti alloys are viable alternatives. It should be noted though that selecting the material prior to the system design aids in to preventing fabrication problems at a later stage (e.g., during drilling, chamfering, rounding, for cutouts, etc.). Thus, the required optical accuracy of the individual components intimately ties in with the selected core materials. ZnSe is an ideal choice as ATR transducer, as it is transparent in a wide MIR spectral range and can be produced at any length and thickness for tailoring the number of internal reflections at reasonable cost. Since ZnSe is stable at pH 5–9, it is suitable for applications in marine environments characterized by moderate pH conditions. However, ZnSe is a brittle crystal and requires protection inside the housing and against the adjacent sample medium. Buffering against the ground plate (i.e., the "H"-shaped part) is provided via a lead sheet. The metal parts encompassing the IRE are designed to withstand high pressures. Since the crystal is fixed in the z-direction, special attention has to be paid to the trapezoidal end facets. Therefore, an appropriate light guiding system is needed to ensure invariant IR radiation coupling into the transducer, while at the same time providing sufficient stability for the end facets, which is herein achieved via especially designed iHWGs. Herein, the iHWGs serve several functions: 1) invariant guiding of IR radiation ensuring perpendicular incidence at the ZnSe end facet; 2) avoiding free space radiation paths; 3) robust protection of the ATR crystal end facets versus vibrations, shock, and temperature; and 4) avoiding additional optical components, such as lenses and so on.

The sensor housing was designed to encompass the sensor cell assembly without any possibility of movement. To avoid any free-space radiation propagation, IR-transparent fibers were used for connecting the laser(s) to the sensor cell and to the detector(s). To ensure heat transport away from the lasers, an appropriate laser mount inside the housing was implemented. This mount is designed, such that several small lasers (e.g., in high heat load housings) can be accommodated in a serial fashion. The tubular housing comprises two symmetric parts assembled into the final system tube.

III. Simulations of System Housing and Sensor Cell

A. Simulations of Water Flow Around the Sensor System

To test the feasibility of the designed system housing at real-world conditions, simulations using parameters relevant to marine environments were conducted. The software package Ansys Fluent Flow (Ansys, 2021) was selected for executing the simulations. An equal distributed water chamber around the housing, with dimensions of 972 × 250 × 125 mm (l × h × w), was applied. For the simulation, an envelope around the housing was applied, followed by removing the housing. The finite element mesh was generated by using tetrahedron elements. The viscous laminar model was selected. Inlet and outlet were defined at both ends with boundary conditions at the inlet defined as a velocity of 4 and 10 m/s, respectively, and a temperature of 400 K. As fluid, water was used and the housing material was selected as steel.

To mimic the water flow around the housing, the device was placed parallel to the water flow (see Fig. 3) followed by simulations, where the housing was placed orthogonal to the water flow (see Fig. 4). While in the parallel orientation, the water pressure is primarily incident at the end facet of the housing (see Fig. 3); in the orthogonal orientation, the water pressure is incident mostly at the crystal (see Fig. 4).

The natural flow velocity of ocean water is up to 4 m/s [41]. In order to determine the sensor behavior at rougher conditions, a water velocity of 10 m/s was also simulated.

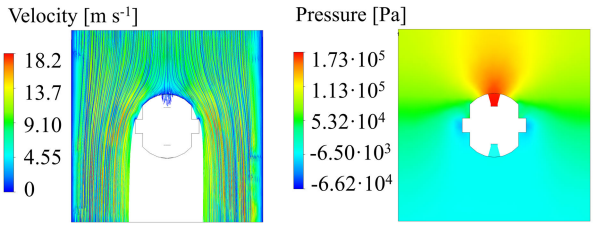

Fig. 4. Simulation of water flow parallel to the ATR crystal.

According to the simulations, at 4 m/s, a pressure of 0.008 bar (800 Pa) is imminent at the front facet of the housing, as shown in Fig. 3(a). With a water flow of 10 m/s, a pressure of 0.5 bar (50 kPa) affects the front facet [see Fig. 3(b)]. Evidently, at both simulation conditions, the pressure at the end facet of the tube is modest.

While at parallel water flow conditions, no damage at the tube and the crystal is expected, the entire sensor housing was turned orthogonal to the water flow (see Fig. 4). For the waterflow perpendicular to the crystal surface, the higher velocity of 10 m/s was selected. The pressure imminent at the ATR crystal surface resulted in 170 kPa (see Fig. 4).

As in Fig. 4, an applied pressure on the crystal of 170 kPa could be observed, while the water flows perpendicular to the tube, further attention on the crystal will be paid. Therefore, this pressure of 170 kPa will be applied onto the (pristine) crystal.

B. Hydrostatic Pressure at the IR-ATR Transducer

With a water flow of 10 m/s perpendicular to the ZnSe crystal, a pressure of 1.7 bar was apparent at the crystal surface (see Fig. 4). To evaluate the stability of the rather delicate ZnSe material, the Von Mises stress was investigated. The simulations were performed using Comsol 5.5 (Comsol Multiphysics GmbH, Sweden). The CAD drawing of the IRE was loaded into the software ensuring direct correlation with the actual prototype. ZnSe was selected as the waveguide material.

Since the crystal is embedded within the sensor cell, the sensing interface has an ellipsoidal shape (see Fig. 1). For simulations of the pressure at the crystal embedded into the housing, the pressure was only applied to the active ellipsoid sensing area (see Fig. 5).

The area of the ellipsoid (see Fig. 2, sensing interface) corresponds to approx. 336 mm^2. To mimic the support of both sloping surfaces provided by the iHWGs and the crystal placed on the ground plate, the bottom side and sloping surfaces of the crystal were implemented as fixed constraints. The finite element mesh was generated by using a physics-controlled mesh with an extra fine size. A force of 57.12 N was applied onto the ellipsoidal ZnSe area, as shown in Fig. 5(a). With an applied pressure of 57.12 N, the maximal Von Mises stress was equal to 54 N/m^2 [see Fig. 5(a)].

In order to evaluate the stability of the crystal, the yield stress of ZnSe at approx. 13 MPa was implemented [26], which is orders of magnitudes higher compared to the Von Mises stress obtained in the present simulations. Therefore, the IR-ATR transducer waveguide should withstand this pressure and no damage of the crystal is anticipated. The maximal displacement derived from these simulations is 0.003 nm.

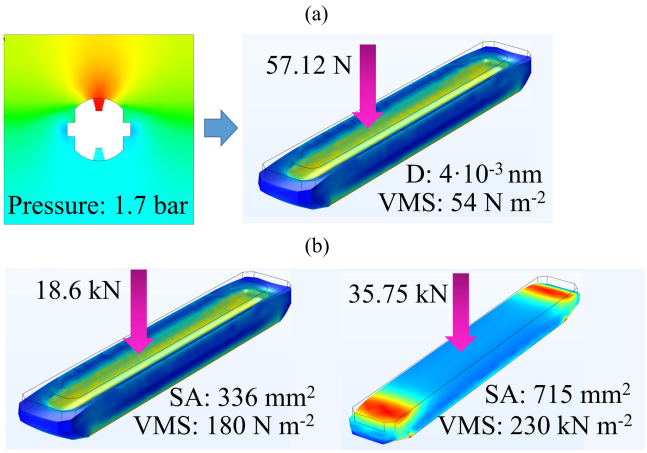

Fig. 5. Simulations of the stability of the ZnSe ATR crystal: abbreviations: SA = surface area, VMS = Von Mises stress, and D = displacement. (a) Pressure on the crystal of 1.7 bar and (b) applying pressure of 50 MPa.

Since an applied pressure of 1.7 bar does should not break the crystal, higher pressures were also evaluated. For that purpose, the elastic limit of ZnSe was taken into account. The elastic limit is defined as the maximal stress per unit area that a solid material can withstand prior to the onset of a permanent deformation [42]. ZnSe has an elastic limit of 55.1 MPa. Therefore, to ensure the crystal does not break, a pressure of 50 MPa was selected. Fig. 5(b) shows the applied pressure of 50 MPa, which is equivalent to an applied force of 18.6 kN at the crystal surface with a contact area of approx. 336 mm^2. The simulations revealed that the Von Mises stress is approx. 16 kN/m^2 with a maximal displacement of 0.01 μm.

To evaluate how much the crystal is protected inside the developed sensor cell and to figure out how the freestanding ZnSe behaves under pressure, a nonembedded ZnSe crystal with the same dimensions as the embedded one was used for simulations. However, it has to be mentioned that the surface area of the nonembedded crystal is higher with a surface area is approx. 715 mm^2 (in comparison to the embedded one with an area of 336 mm^2), as shown in Fig. 5(b). In the nonembedded crystal, a force of 50 MPa was also applied. The pressure of 50 MPa correlates to a force of 35.75 kN, which was applied at the crystal surface. For the IRE not implemented into the housing, the Von Mises stress was approx. 230 kN/m^2 with a maximal displacement of 0.02 μm. The Von Mises stress is lower compared to the yield stress, and it is anticipated that the crystal will not break. As evident in Fig. 5, the nonembedded IRE has higher Von Mises stress compared to the embedded one. Interestingly, the Von Mises stress is approximately 15-times lower for the embedded crystal compared to the freestanding crystal. Furthermore, the maximal displacement is lower for the embedded crystal, as the pressure is not applied onto the edges, which are the most fragile part of the ATR waveguide.

IV. Experiment

A. Chemicals

Absolute ethanol (96%) has been purchased from VWR Chemicals, Germany. All solutions were freshly prepared in

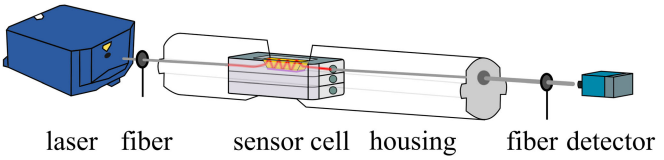

Fig. 6. Laboratory prototype experimental setup: light emitted from an EC-QCL propagates *via* hollow-core fiberoptic cables to the IR-ATR transducer assembly located in the sensor system housing and from there to the detector.

ultrapure water (18.0 MΩ cm, Elga Labwater; VWS Deutschland, Germany).

B. Laboratory Setup for Ethanol Measurements

For experimental flexibility, the laboratory sensor setup shown in Fig. 6 does not use single-emission QCLs and thermopile detectors readily integrated into the tube but external laser light source and detector components.

The laboratory setup consists of a water-cooled external-cavity (EC)-QCL (MIRcat, Daylight Solutions, USA) serving as the IR light source comprising four individual broadly tunable EC-QCLs covering a wavelength range between 1900 and 900 cm^{-1}. The wavelength range, which is used in this study, is 1100–1020 cm^{-1} and corresponds to the characteristic vibrational signature of ethanol serving as the test analyte. The benefit of using a broadly tunable laser for test measurement is to obtain a broad vibrations spectrum instead of a single measurement point. Knowing the spectral behavior and the sensor response, single-wavelength measurements can be conducted during future research tailored to a specific measurement scenario and analyte of interest. As detector, a TE-cooled MCT detector (PCI-3TE-13/MIP-10-1M-F-M4, Vigo Systems S.A., Poland) was used during laboratory measurements. During the prototype measurements, the IR-ATR transducer assembly was indeed located inside the sensor system housing. The IR radiation from the EC-QCL to the sensor assembly and to the detector was guided via hollow-core fibers. These fibers are slightly longer than the ones in the final configuration with the QCL(s) and the detector(s) located inside the tube. However, as these fibers have low optically losses, slightly longer coupling fibers do not affect the obtained results. The first fiber couples the IR radiation to the sensor cell via the iHWG coupler. IR radiation then propagates along the IRE and is guided via the second iHWG coupler via fiber connection to the detector.

Ethanol–water mixture was applied at the ZnSe crystal surface with a sample volume of 1 mL. Each sample was analyzed three times from lower to higher concentrations with appropriate cleaning steps in between each measurement.

Data acquisition was performed using a homemade LabView-based GUI (National Instrument Corporation, Austin, USA) and digitized via NI-DAQmx (National Instruments Corporation, USA). The obtained transmission spectra were imported into Origin (OriginLab 2019b, USA) and a fast Fourier transform (FFT) filter was applied and absorbance spectra were calculated. As a background, the spectrum of deionized water was used. Baseline correction

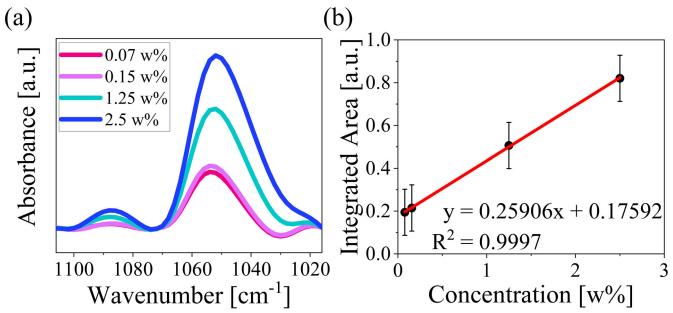

Fig. 7. Exemplary concentration-dependent ethanol-in-water IR spectra (a) and corresponding calibration (b) determined via IR-ATR laser spectroscopy using the developed sensor system.

and peak integration were conducted in the range of 1016 and 1071 cm^{-1} using the software package Orange by Quasar. The standard deviation was obtained by averaging three spectra.

V. Laboratory Experiments: Ethanol-in-Water Mixture for Sensor Validation

For comparability of the sensor cell located in the housing with an assembly without housing used during previous studies [31], the same experimental conditions and the same analyte system—ethanol in water—were selected. Besides, ethanol is indeed a relevant small molecule in a variety of scenarios, e.g., in ethanol–gasoline mixtures for combustion engines and so on [43]. The laboratory laser light source and the applied detector are similar to previous studies [31].

Fig. 7(a) shows the obtained ethanol-in-water absorption spectra. Each ethanol concentration had been analyzed three times from the lowest to the highest concentrations avoiding cross-contamination; the average of three spectra are shown. The characteristic vibrational signature of ethanol at 1046 cm^{-1} corresponds to the CO stretching vibration [44]. For data evaluation, the peak area was integrated and plotted versus the concentration. Next to the absorption spectra, the corresponding calibration function of the ethanol–water mixture is provided [see Fig. 7(b)]. A linear range between 0.07 and 2.5 w% was obtained. The limit of detection (LOD) was calculated based on the three-sigma-criterion at 0.045 w%.

Since the same laser light source, analyte, and detector were used in the present study, a comparison to previously obtained results is facilitated [31]. It is evident that the LOD in the present study had been lowered from 0.05 to 0.045 w%. Clearly, avoiding any free-space optical path leads to an improved LOD. At the same time, an exceedingly compact and robust sensor system design is obtained. The obtained sensitivity along with the robust overall system design provides access to a wide range of sensing scenarios in harsh environments. Especially, the cylindrical system housing facilitates future in-field studies.

VI. Conclusion

The presented IR-ATR transducer assembly packaged into an exceedingly robust and compact tubular system provides an excellent sensor concept for deployment at harsh environmental conditions. The sensor concept is based on MIR

laser-based spectroscopy enabling the analysis of molecular constituents in harsh environments, e.g., marine systems. The entire sensor system is designed to be immersed into marine environments for performing molecular analysis. The sensor cell is embedded into a robust housing facilitating the usage of conventional low-cost ZnSe crystals as active transducers. Using innovative optical coupling concepts based on hollow core fibers and iHWGs allows avoiding any free-space optical pathways and any conventional optical components within the entire sensor system. Therefore, there are no components within the system that could be subject to misalignment at real-world conditions. Simulations have demonstrated that the sensor system design and the ATR crystal transducer interface are suitable for real-world applications at elevated pressures. To test the analytical feasibility of the designed sensor system, ethanol-in-water was quantitatively determined serving as a model analyte. It was shown that the developed sensor concept provides improved LODs versus previously demonstrated QCL-based sensing devices while improving the robustness of the system and packaging into an exceedingly compact tube-shaped format with a diameter of 5 cm.

Acknowledgment

The authors acknowledge the Workshop at Ulm University for support in IR-ATR transducer assembly fabrication. They also thank Mr. Novica Vidovic and Dr. Markus Naegele, OptoPrecision, Germany, for design support and fabrication of the tubular sensor housing.

References

[1] P. Kurán and L. Sojak, "Environmental analysis of volatile organic compounds in water and sediment by gas chromatography," *J. Chromatography A*, vol. 733, nos. 1–2, pp. 119–141, May 1996, doi: 10.1016/0021-9673(95)01121-8.

[2] R. Stach, B. Pejcic, E. Crooke, M. Myers, and B. Mizaikoff, "Mid-infrared spectroscopic method for the identification and quantification of dissolved oil components in marine environments," *Anal. Chem.*, vol. 87, no. 24, pp. 12306–12312, Dec. 2015, doi: 10.1021/acs.analchem.5b03624.

[3] C. Heath, M. Myers, and B. Pejcic, "The effect of pressure and temperature on mid-infrared sensing of dissolved hydrocarbons in water," *Anal. Chem.*, vol. 89, no. 24, pp. 13391–13397, Dec. 2017, doi: 10.1021/acs.analchem.7b03623.

[4] U. R. Sumaila et al., "Impact of the deepwater horizon well blowout on the economics of US Gulf fisheries," *Can. J. Fisheries Aquatic Sci.*, vol. 69, no. 3, pp. 499–510, Mar. 2012, doi: 10.1139/f2011-171.

[5] B. Pejcic, P. Eadington, and A. Ross, "Environmental monitoring of hydrocarbons: A chemical sensor perspective," *Environ. Sci. Technol.*, vol. 41, no. 18, pp. 6333–6342, Sep. 2007, doi: 10.1021/es0704535.

[6] H. Chen, M. Buric, P. R. Ohodnicki, J. Nakano, B. Liu, and B. T. Chorpening, "Review and perspective: Sapphire optical fiber cladding development for harsh environment sensing," *Appl. Phys. Rev.*, vol. 5, no. 1, Mar. 2018, Art. no. 011102, doi: 10.1063/1.5010184.

[7] A. Ghosh, C. Zhang, S. Q. Shi, and H. Zhang, "High-temperature gas sensors for harsh environment applications: A review," *CLEAN-Soil, Air, Water*, vol. 47, no. 8, Aug. 2019, Art. no. 1800491, doi: 10.1002/clen.201800491.

[8] I. Leifer et al., "State of the art satellite and airborne marine oil spill remote sensing: Application to the BP deepwater horizon oil spill," *Remote Sens. Environ.*, vol. 124, pp. 185–209, Sep. 2012, doi: 10.1016/j.rse.2012.03.024.

[9] J. Beyer, H. C. Trannum, T. Bakke, P. V. Hodson, and T. K. Collier, "Environmental effects of the deepwater horizon oil spill: A review," *Mar. Pollut. Bull.*, vol. 110, no. 1, pp. 28–51, Sep. 2016, doi: 10.1016/j.marpolbul.2016.06.027.

[10] M. Allers et al., "Real-time remote detection of airborne chemical hazards—An unmanned aerial vehicle (UAV) carrying an ion mobility spectrometer," *IEEE Sensors J.*, vol. 23, no. 15, pp. 16562–16570, Aug. 2023, doi: 10.1109/JSEN.2023.3287448.

[11] L. Dong et al., "Studying soil moisture and temperature on the Tibetan Plateau: Initial results of an integrated, multiscale observatory," *IEEE Geosci. Remote Sens. Mag.*, vol. 8, no. 3, pp. 18–36, Sep. 2020, doi: 10.1109/MGRS.2019.2924678.

[12] M. Ams et al., "Fibre optic temperature and humidity sensors for harsh wastewater environments," in *Proc. 11th Int. Conf. Sens. Technol. (ICST)*, Dec. 2017, pp. 1–3, doi: 10.1109/ICSensT.2017.8304493.

[13] L. Procópio, "The role of biofilms in the corrosion of steel in marine environments," *World J. Microbiol. Biotechnol.*, vol. 35, no. 5, p. 73, May 2019, doi: 10.1007/s11274-019-2647-4.

[14] L. Tomanek, "Proteomics to study adaptations in marine organisms to environmental stress," *J. Proteomics*, vol. 105, pp. 92–106, Jun. 2014, doi: 10.1016/j.jprot.2014.04.009.

[15] P. Cunat, "Selection and use of stainless steels in water systems," Int. Molybdenium Assoc. (IMOA), Brussels, Euro-Inox, Tech. Rep., 2003.

[16] D. Wang, J. Lee, K. Holland, T. Bibby, S. Beaudoin, and T. Cale, "Von Mises stress in chemical-mechanical polishing processes," *J. Electrochemical Soc.*, vol. 144, no. 3, pp. 1121–1127, Mar. 1997, doi: 10.1149/1.1837542.

[17] N. W. Tschoegl, "Failure surfaces in principal stress space," *J. Polym. Sci. C, Polym. Symposia*, vol. 32, no. 1, pp. 239–267, Mar. 2007, doi: 10.1002/polc.5070320113.

[18] A. R. Boccaccini, G. Ondracek, P. Mazilu, and D. Windelberg, "On the effective Young's modulus of elasticity for porous materials: Microstructure modelling and comparison between calculated and experimental values," *J. Mech. Behav. Mater.*, vol. 4, no. 2, pp. 119–128, Mar. 1993, doi: 10.1515/jmbm.1993.4.2.119.

[19] Britannica and TE Encyclopedia, *Shear Stress*, The IUPAC Compendium of Chemical Terminology, USA, 2008.

[20] A. Merdji, B. B. Bouiadjra, T. Achour, B. Serier, B. O. Chikh, and Z. O. Feng, "Stress analysis in dental prosthesis," *Comput. Mater. Sci.*, vol. 49, no. 1, pp. 126–133, Jun. 2010, doi: 10.1016/j.commatsci.2010.04.035.

[21] O. Giraldo-Londoño and G. H. Paulino, "A unified approach for topology optimization with local stress constraints considering various failure criteria: Von Mises, Drucker–Prager, Tresca, Mohr–Coulomb, Bresler–Pister and Willam–Warnke," *Proc. Roy. Soc. A, Math., Phys. Eng. Sci.*, vol. 476, no. 2238, Jun. 2020, Art. no. 20190861, doi: 10.1098/rspa.2019.0861.

[22] O. Eraslan, M. Sevimay, A. Usumez, and G. Eskitascioglu, "Effects of cantilever design and material on stress distribution in fixed partial dentures—A finite element analysis," *J. Oral Rehabil.*, vol. 32, no. 4, pp. 273–278, Apr. 2005, doi: 10.1111/j.1365-2842.2004.01429.x.

[23] R. Jackson, I. Chusoipin, and I. Green, "A finite element study of the residual stress and deformation in hemispherical contacts," *J. Tribol.*, vol. 127, no. 3, pp. 484–493, Jul. 2005, doi: 10.1115/1.1843166.

[24] I. S. Burmistrov, I. V. Gornyi, V. Y. Kachorovskii, M. I. Katsnelson, J. H. Los, and A. D. Mirlin, "Stress-controlled Poisson ratio of a crystalline membrane: Application to graphene," *Phys. Rev. B, Condens. Matter*, vol. 97, no. 12, Mar. 2018, Art. no. 125402, doi: 10.1103/physrevb.97.125402.

[25] R. Goodall and A. Mortensen, "Porous metals," in *Physical Metallurgy*. Amsterdam, The Netherlands: Elsevier, 2014, pp. 2399–2595, doi: 10.1016/B978-0-444-53770-6.00024-1.

[26] I. Yonenaga, K. Watanabe, S. Itoh, S. Fujiwara, and K. Yoshino, "Yield strength and dislocation mobility in plastically deformed ZnSe," *Phys. B, Condens. Matter*, vols. 376–377, pp. 771–774, Apr. 2006, doi: 10.1016/j.physb.2005.12.193.

[27] L. Hvozdara, N. Pennington, M. Kraft, M. Karlowatz, and B. Mizaikoff, "Quantum cascade lasers for mid-infrared spectroscopy," *Vibrational Spectrosc.*, vol. 30, no. 1, pp. 53–58, Sep. 2002, doi: 10.1016/S0924-2031(02)00038-3.

[28] J. Haas and B. Mizaikoff, "Advances in mid-infrared spectroscopy for chemical analysis," *Annu. Rev. Anal. Chem.*, vol. 9, no. 1, pp. 45–68, Jun. 2016, doi: 10.1146/annurev-anchem-071015-041507.

[29] T. Schädle and B. Mizaikoff, "Mid-infrared waveguides: A perspective," *Appl. Spectrosc.*, vol. 70, no. 10, pp. 1625–1638, Oct. 2016, doi: 10.1177/0003702816659668.

[30] A. Teuber and B. Mizaikoff, "Cascade laser infrared spectroscopy," in *Encyclopedia of Analytical Chemistry*. Hoboken, NJ, USA: Wiley, 2021, pp. 1–45, doi: 10.1002/9780470027318.a9751.

[31] A. Teuber, R. Stach, J. Haas, and B. Mizaikoff, "Innovative substrate-integrated hollow waveguide coupled attenuated total reflection sensors for quantum cascade laser based infrared spectroscopy in harsh environments," *Appl. Spectrosc.*, vol. 76, no. 1, pp. 132–140, 2021, doi: 10.1177/00037028211064331.

[32] J. Fahrenfort, "Attenuated total reflection: A new principle for the production of useful infra-red reflection spectra of organic compounds," *Spectrochimica Acta*, vol. 17, no. 7, pp. 698–709, Jan. 1961, doi: 10.1016/0371-1951(61)80136-7.

[33] N. J. Harrick, "Total internal reflection and its application to surface studies," *Ann. New York Acad. Sci.*, vol. 101, no. 3, pp. 928–959, Jan. 1963, doi: 10.1111/j.1749-6632.1963.tb54948.x.

[34] M. Milosevic, "Internal reflection and ATR spectroscopy," *Appl. Spectrosc. Rev.*, vol. 39, no. 3, pp. 365–384, Dec. 2004, doi: 10.1081/asr-200030195.

[35] L. A. Averett, P. R. Griffiths, and K. Nishikida, "Effective path length in attenuated total reflection spectroscopy," *Anal. Chem.*, vol. 80, no. 8, pp. 3045–3049, Apr. 2008, doi: 10.1021/ac7025892.

[36] T. G. Mayerhöfer, S. Pahlow, and J. Popp, "Recent technological and scientific developments concerning the use of infrared spectroscopy for point-of-care applications," *Spectrochimica Acta A, Mol. Biomolecular Spectrosc.*, vol. 251, Apr. 2021, Art. no. 119411, doi: 10.1016/j.saa.2020.119411.

[37] P. R. Griffiths, "Fourier transform infrared spectrometry," *Science*, vol. 222, no. 4621, pp. 297–302, Oct. 1983, doi: 10.1126/science.6623077.

[38] B. P. Banerjee, S. Raval, T. J. Maslin, and W. Timms, "Development of a UAV-mounted system for remotely collecting mine water samples," *Int. J. Mining, Reclamation Environ.*, vol. 34, no. 6, pp. 385–396, Jul. 2020, doi: 10.1080/17480930.2018.1549526.

[39] D. J. Stefanik, L. E. Friedman, and J. R. Finnerty, "Collecting, rearing, spawning and inducing regeneration of the starlet sea anemone, nematostella vectensis," *Nature Protocols*, vol. 8, no. 5, pp. 916–923, May 2013, doi: 10.1038/nprot.2013.044.

[40] A. Wilk et al., "Substrate-integrated hollow waveguides: A new level of integration in mid-infrared gas sensing," *Anal. Chem.*, vol. 85, no. 23, pp. 11205–11210, Dec. 2013, doi: 10.1021/ac402391m.

[41] C. Cenedese and A. L. Gordon. *Ocean Current*. Encyclopedia Britannica. Accessed: Apr. 20, 2023. [Online]. Available: https://www.britannica.com/science/ocean-current

[42] J. C. Shedd and R. L. Ingersol, "The elastic modulus and elastic limit of rubber and their relation to change of temperature," *Phys. Rev.*, vol. 19, no. 2, pp. 107–116, Aug. 1904, doi: 10.1103/physrevseriesi.19.107.

[43] L. R. Lynd, "Overview and evaluation of fuel ethanol from cellulosic biomass: Technology, economics, the environment, and policy," *Annu. Rev. Energy Environ.*, vol. 21, no. 1, pp. 403–465, Nov. 1996, doi: 10.1146/annurev.energy.21.1.403.

[44] E. K. Plyler, "Infrared spectra of methanol, ethanol, and n-propanol," *J. Res. Nat. Bur. Standards*, vol. 48, no. 4, p. 281, Apr. 1952, doi: 10.6028/jres.048.036.

Andrea Teuber was born in Augsburg, Germany. She received the bachelor's degree in chemistry from the Institute of Analytical and Bioanalytical Chemistry (IABC), Ulm University, Ulm, Germany, in 2017, focused on researching gas phase laser spectroscopy applied in health care scenarios, the master's degree in chemistry from IABC, in 2019, focused on liquid phase midinfrared laser spectroscopy, under the supervision of Prof. Boris Mizaikoff. She is pursuing the Ph.D. degree with IABC, under the supervision of Prof. Boris Mizaikoff, focused on the development of IR-ATR laser-based sensors for harsh environments and on improved waveguide technologies for miniaturized sensor concepts, including sensor system simulations and advanced application scenarios.

Boris Mizaikoff (Member, IEEE) is a Chaired Professor and the Director of the Institute of Analytical and Bioanalytical Chemistry (IABC), Ulm University, Ulm, Germany, with previous appointments at the Vienna University of Technology, Vienna, Austria, and Georgia Institute of Technology, Atlanta, GA, USA. Since 2021, he has been the Director of the Hahn-Schickard Institute for Microanalysis Systems, Ulm. He is the author/coauthor of 400+ peer-reviewed publications, 18 patents, and 150+ plenary, keynote, and invited contributions at scientific conferences. His research interests focus on optical sensors, biosensors, and biomimetic sensors in the mid-infrared spectral range, system miniaturization, and integration based on micro- and nanofabrication, multifunctional (nano)analytical platforms, development of biomolecular/biomimetic molecular recognition architectures, multivariate data evaluation, and applications in environmental analytics, process analysis, and biomedical/clinical diagnostics.